# Functional Platform for Controlled Subcellular Distribution of Carbon Nanotubes

**Maged F. Serag,[†,‡,¶,*] Noritada Kaji,[†,‡] Enrica Venturelli,[§] Yukihiro Okamoto,[†,‡] Kazuyoshi Terasaka,[∥] Manabu Tokeshi,[†,‡] Hajime Mizukami,[∥] Kevin Braeckmans,[⊥,#] Alberto Bianco,[§] and Yoshinobu Baba[†,‡,○]**

[†]Department of Applied Chemistry, Graduate School of Engineering, and [‡]FIRST Research Center for Innovative Nanodevices, Nagoya University, Japan, [¶]Department of Pharmacognosy, Faculty of Pharmacy, Zagazig University, Egypt, [§]Centre National de la Recherche Scientifique, Institut de Biologie Moléculaire et Cellulaire, UPR 9021 Immunologie et Chimie Thérapeutiques, Strasbourg, France, [∥]Department of Pharmacognosy, Graduate School of Pharmaceutical Sciences, Nagoya City University, Japan, [⊥]Biophotonic Imaging Group, Laboratory of General Biochemistry and Physical Pharmacy, Ghent University, Harelbekestraat 72, B-9000 Ghent, Belgium, [#]Centre for Nano- and Biophotonics, Ghent University, Belgium, and [○]National Institute of Advanced Industrial Science and Technology (AIST), Takamatsu, Japan

**ABSTRACT** As nanoparticles can cross different cellular barriers and access different tissues, control of their uptake and cellular fate presents a functional approach that will be broadly applicable to nanoscale technologies in cell biology. Here we show that the trafficking of single-walled carbon nanotubes (SWCNTs) through various subcellular membranes of the plant cell is facilitated or inhibited by attaching a suitable functional tag and controlling medium components. This enables a unique control over the uptake and the subcellular distribution of SWCNTs and provides a key strategy to promote their cellular elimination to minimize toxicity. Our results also demonstrate that SWCNTs are involved in a carrier-mediated transport (CMT) inside cells; this is a phenomenon that scientists could use to obtain novel molecular insights into CMT, with the potential translation to advances in subcellular nanobiology.

**KEYWORDS:** plant cell · single-walled carbon nanotubes · fluorescein isothiocyanate · diffusional mobility · subcellular distribution

Functionalized carbon nanotubes (*f*-CNTs) have been shown to traverse different cellular barriers including mammalian,[1−3] bacterial,[3,4] and plant[5,6] cells. While many studies focused on toxicity issues,[7] biomolecular delivery,[5,8−10] and investigating their uptake mechanism,[3,6,10] efforts to control their subcellular distribution are still needed. Controlling the subcellular distribution of *f*-CNTs is of a practical and fundamental importance for intracellular labeling and imaging, genetic transformation, and for enhancing our knowledge of cell biology. A significant advantage that single-walled carbon nanotubes (SWCNTs) have over multiwalled carbon nanotubes (MWCNTs) in cell biology studies is that their diameters approach the size of biomolecules and therefore they could potentially participate in subcellular processes if properly labeled with a suitable functional tag. Although covalent attachment of these tags could provide a stable conjugate, physical adsorption is often superior in terms of getting a high loading ratio.[11]

As a technical prerequisite to subcellular distribution studies, a suitable detection technology should be available to track *f*-CNTs in different cell compartments. Although, several technologies such as confocal detection[3−6] and transmission electron microscopy (TEM)[12,13] have been successfully employed to track *f*-CNTs, their reliability is limited under certain experimental conditions. For example, by mere imaging it cannot be excluded that the detected fluorescence comes from fluorophore labels that are released from the *f*-CNTs. TEM studies also may result in a false-negative interpretation because of considerable similarity in TEM images of CNTs and natural cell structures. Photobleach measurements have been the method of choice for determining the diffusional mobility and mobile fraction for fluorophores in solution.[14,15] Therefore, fluorescence recovery after photobleaching (FRAP)[14] could provide more information about subcellular localization of *f*-CNTs by distinguishing free fluorophores from fluorophore-labeled CNTs based on a difference in mobility.

## RESULTS AND DISCUSSION

**Vacuolar Uptake of Single-Walled Carbon Nanotubes (SWCNTs).** To investigate the behavior of SWCNTs inside living cells we used suspended cells of the genetically recalcitrant plant model *Catharanthus roseus*.[6,16] Short carboxylated SWCNTs (Figure 1a and SI, Figure S1) were prepared by ultrasonic-assisted chemical oxidative cutting and then fluorescently labeled with fluorescein

* Address correspondence to magedserag@yahoo.com.

Received for review September 16, 2011 and accepted October 7, 2011.

**Published online October 07, 2011**
**10.1021/nn2035654**

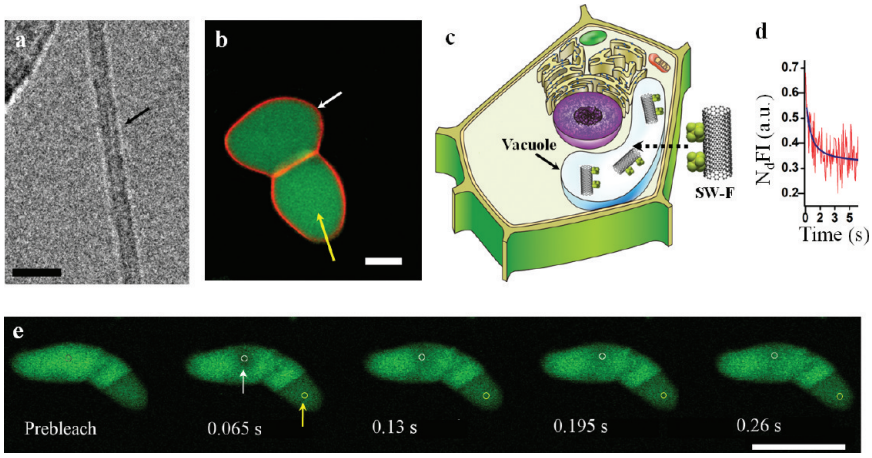


**Figure 1. Characterization of SW-F accumulation in C. roseus vacuoles. (a) A TEM micrograph of SW-F (diameter ~ 1.4 nm). Scale bar: 5 nm. (b) Confocal microscopy image of C. roseus cells incubated with 5 $\mu$g/mL SW-F. The white arrow indicates the cell membrane stained with FM4−64 dye, while the yellow arrow indicates green fluorescence of SW-F accumulated in a large vacuole (SI, Figures S2a,b show bright field image of C. roseus cells). Scale bar: 20 $\mu$m. (c) Plant cell schematic figure showing trafficking of SW-F into a cell vacuole. (d,e) Qualitative FRAP analysis of the vacuolar accumulation of SW-F. The small region (circles) in the vacuole was photobleached. The subsequent recovery of fluorescence in this region was monitored by time-lapse imaging for at least 15 s. Numbers at the bottom indicate the time after photobleaching in seconds. Scale bar: 50 $\mu$m. The FRAP analyses of cells incubated with FITC are presented in SI, Figure S3. The plot of the FRAP curve (d) illustrates the first 5 s of the FRAP experimental (red line) and FRAP simulation (blue line) recoveries. The FRAP curve was extracted from the postbleach images by defining the bleach ROI (white circle) and the reference ROI (yellow circle marked by a yellow arrow in (e)). To compensate for photobleaching, the normalized difference of the fluorescence intensity ($N_dFI$) between the bleach and the reference ROIs was used (see Experimental Section). The final recovery curve after photobleaching correction was an exponentially decaying function for $N_dFI$. The blue line shows the best fit of the FRAP Kapitza model to the experimental recovery curve.**

isothiocyanate (FITC) *via* $\pi$-stacking[17,18] (hereafter abbreviated as SW-F). Following incubation with FITC or SW-F, fluorescence signals were exclusively localized in the cell vacuoles (Figure 1b,c; SI, Figure S2). To confirm that the intracellular distribution of the fluorescence signal reported the SW-F localization and was not due to free FITC, we carried out FRAP analyses on both FITC and SW-F treated cells (Figure 1d,e). The diffusion coefficient ($D_{eff}$) of SW-F in cell vacuoles ranged between 20 and 70 $\mu m^2/s$ and was considerably slower than that of free unbound FITC molecules ($D_{eff}$ = 120−150 $\mu m^2/s$) (SI, Figure S3). This indicated the accumulation of SW-F inside cell vacuoles.

**Cytoplasmic Accumulation of Single-Walled Carbon Nanotubes Tagged with FITC (SW-F).** In view of several reports of vacuolar accumulation of fluorescent anions,[19−21] we decided to examine the effect of probenecid (an inhibitor of carrier-mediated transport (CMT) in plant and mammalian cells[21]) on the vacuolar accumulation of SW-F. Notably, FITC enters cells predominantly *via* passive diffusion and is rapidly transported across the vacuolar membrane *via* CMT.[19] Interestingly, probenecid inhibited the vacuolar uptake of SW-F demonstrating that FITC controlled the subcellular distribution of SWCNTs and resulted in their cytoplasmic accumulation (Figure 2a,b). Fifty-second sampling of FRAP in the cytoplasm of SW-F treated cells resulted in a diffusion rate about 6−7 times slower than that of free FITC (Table 1, Figure 2c,f, and SI, Figure S4a). This further confirmed that the fluorescence signal in the cytoplasm was attributable to SW-F. Moreover, the mobile fraction of SW-F in the cytoplasm was about 2-fold larger than the mobile fraction of FITC (Table 1 and Figure 2g). This indicated that stacking of FITC on the SWCNT surfaces alleviated to some extent the interaction of the FITC molecules with cytoplasmic components so that a relatively larger percentage of SW-F was able to diffuse freely.

**Intranuclear Release of FITC from Single-Walled Carbon Nantoubes Surfaces.** The accumulation of SW-F in cytoplasm increased the chances to enter a cell nucleus (SI, Figures S4b,S5). The dynamic behavior of macromolecules in cellular fluids is known to be basically controlled by physical constraints imposed by their size.[14] Accordingly, SW-F encountered a significant size diffusion barrier in cytoplasm compared to FITC. If FITC detaches from the SWCNT surfaces, then the measured overall diffusion coefficient would accordingly increase. In the nucleoplasm, the measured diffusion of SW-F was only two- to 3-fold slower than that of FITC (*cf.* 6- to 7-fold in the cytoplasm; Table 1 and Figure 2d, f). Considering the highly dense nature of the nucleoplasm, this suggested a possible intranuclear FITC release (see Supplementary Text of Figure S4). Because FITC stacking on SWCNTs elevated the mobile fraction estimated from the cytoplasmic FRAP results, the similarity of the mobile fractions in the nucleoplasm of FITC and SW-F treated cells (Figure 2g) added further evidence about the phenomenon of FITC release. The highly basic nature of nuclear proteins such as fibrillarin[22,23] and nucleolin[24] may account for a stronger binding of the negatively charged SWCNTs to the nucleoplasm

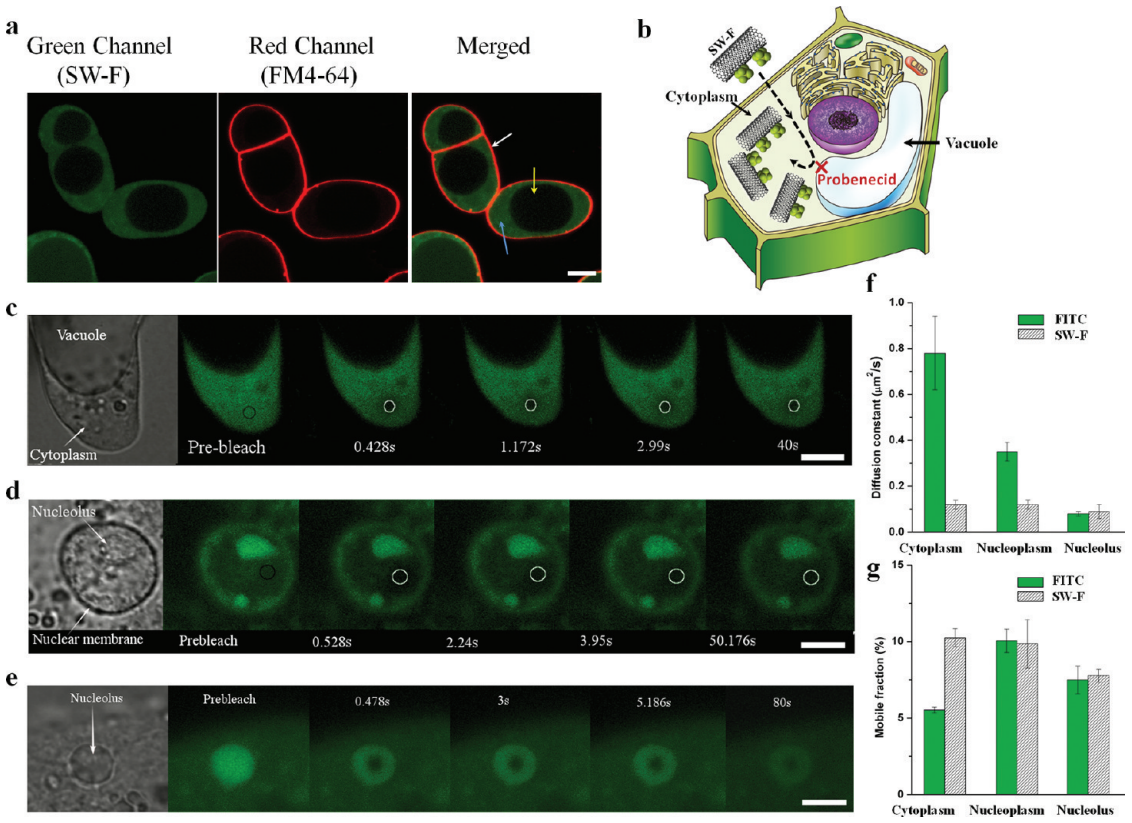


**Figure 2. Characterization of SW-F accumulation in C. roseus cytoplasm and nucleus. (a) Confocal microscopy images of C. roseus cells incubated with 5 $\mu$g/mL SW-F and 5 mM probenecid. The white arrow indicates the cell membrane stained with FM4−64 dye, while the yellow arrow indicates the cell vacuole. The blue arrow indicates the cytoplasm. Scale bar: 10 $\mu$m. (b) Plant cell schematic figure showing trafficking of SW-F into cell cytoplasm where CMT into a cell vacuole is inhibited *via* probenecid. (c−e) Qualitative FRAP analysis of the accumulation of SW-F in cytoplasm, nucleoplasm and nucleolus respectively. The small region (circles) was photobleached. The subsequent recovery of fluorescence in this region was monitored by time-lapse imaging as indicated in Table 1. Scale bars: (c) 5 $\mu$m; (d,e) 2 $\mu$m. Numbers at the bottom indicate the time after photobleaching in seconds. The FRAP analyses of cells incubated with FITC are presented in SI, Figure S4. (f,g) Diffusion coefficients ($\mu$m$^2$/s) and mobile fractions (%) as estimated on the basis of diffusion data of FITC and SW-F accumulated in cytoplasm, nucleoplasm, and nucleolus of C. roseus cells. Results are presented as mean ± s.e.m.**

**TABLE 1. Diffusion Coefficients and Mobile Fractions of FITC and SW-F in Different Subcellular Locations of C. roseus Cells Obtained Using FRAP[a]**

| | Diffusion coefficient (μm²/s) Mobile fraction (%) | | | |
|---|---|---|---|---|
| Subcellular location | Cytoplasm | | Nucleoplasm | Nucleolus |
| FRAP sampling time | 10 s | 50 s | 100 s | 100 s |
| FITC | 0.79±0.16<br>5.5±0.2 | | 0.35±0.05<br>9.6±0.7 | 0.08±0.01<br>7.1±0.9 |
| SW-F | | 0.12±0.02<br>10.3±0.59 | 0.13±0.02<br>9.4±1.5 | 0.09±0.03<br>7.4±0.4 |

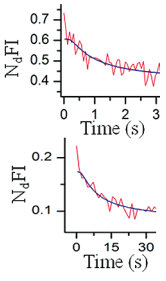


[a] A fast form of diffusion (primary diffusion) can be calculated by analyzing photobleach recoveries during 10 s in the cytoplasm, as indicated; the slower form of diffusion (secondary diffusion) is basically represented by the overall fluorescence recovery within 50 s. Plots on the right illustrate FRAP experimental recoveries (red lines) and FRAP simulation recoveries (blue lines) in cytoplasm, and show the first 3 and 30 s recoveries of primary and secondary diffusions, respectively. The blue lines show the best fit of the FRAP Kapitza model to the experimental recovery curves (see Experimental Section). $N_d$FI: Normalized difference of fluorescence intensity. FITC and SW-F shared the same FRAP values in cytoplasm during the 10 s recovery period. This indicated that these values represented free FITC in both FITC and SW-F treated cells. A major part of the FITC interacted with cytoplasm and only a minor fraction (~5.5%) diffused freely. This mobile fraction increased to ~10.3% in SW-F treated cells. Results are presented as mean ± s.e.m.

compared to cytoplasm and, hence, the release of the stacked molecular species would be facilitated. The released FITC was hypothesized to have then accumulated in the nucleolus based on the similarity of FRAP data from FITC and SW-F treated cells (Figure 2e−g). Considering their small size, SWCNTs had no effect on the

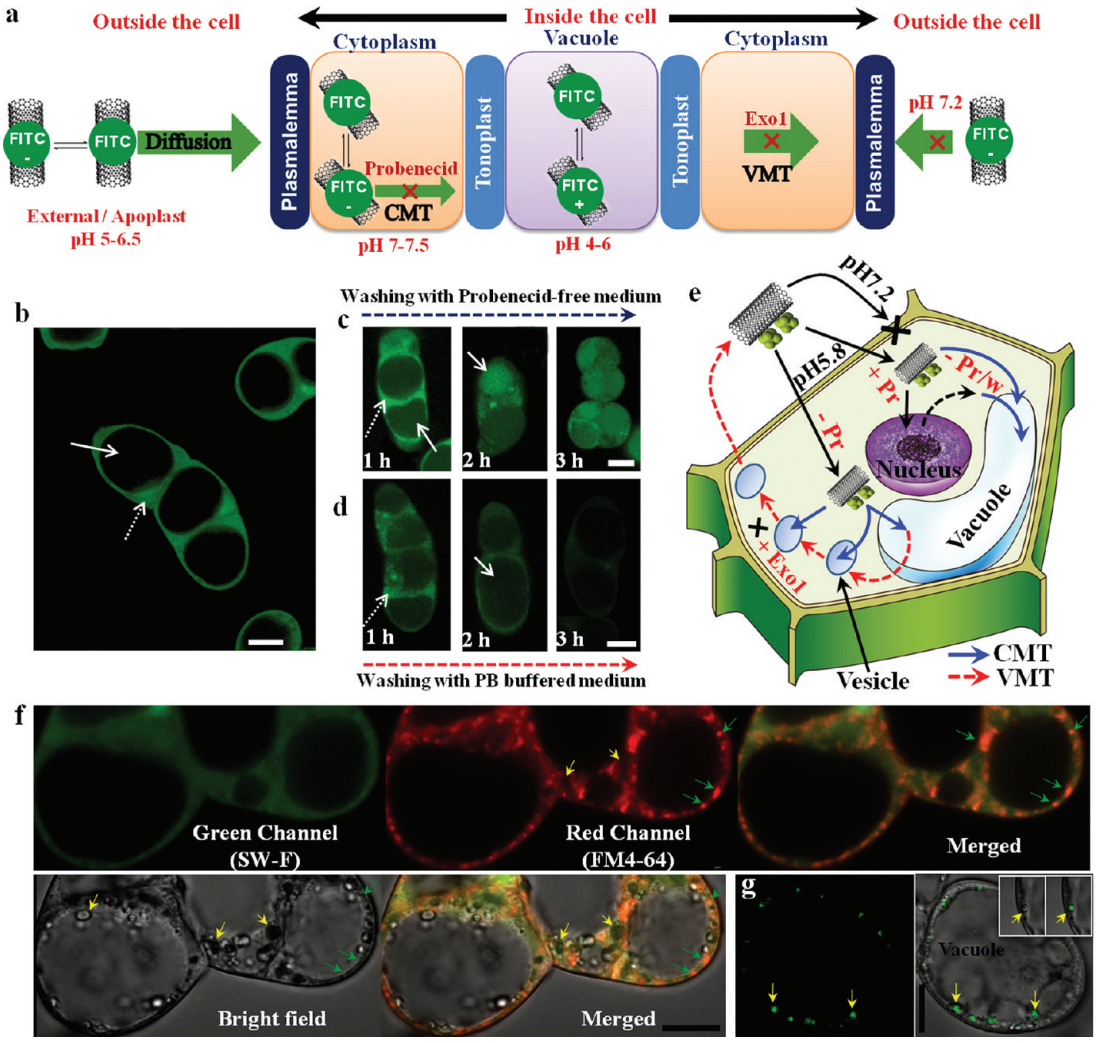


**Figure 3. Controlled subcellular distribution of SW-F in C. roseus cells. (a) Overview of the pathways for SW-F intracellular transport. SI, Figure S9 shows the protonic equilibria of FITC in an aqueous solution. At external pH of 5.0−6.5, the neutral form of FITC entered the cell by diffusion. In the cytoplasm (pH 7.0−7.5), most of the neutral FITC dissociated into its anionic form. The FITC was then transported into the vacuole by probenecid-sensitive CMT. Exo1 regulated FITC trafficking toward plasma membrane through interference with the VMT. (b) Confocal microscopy image of C. roseus cell incubated in nutrient medium supplemented with 5 mM probenecid and 5 $\mu$g/mL SW-F. Probenecid inhibited vacuolar accumulation of SW-F in the vacuole (solid arrow) and consequently promoted their cytoplasmic accumulation (dotted arrow). (c) Redistribution of SW-F into cell vacuole (solid arrow) upon washing probenecid-treated cells with probenecid-free medium (pH = 5.8). Scale bar: 20 $\mu$m. The quantitative FRAP analysis of the redistributed SW-F is displayed in SI, Figure S10a. The mean fluorescence intensity data are presented in SI, Figure S10b. (d) Progressive clearance of SW-F from cytoplasm (dotted arrow) upon washing with phosphate buffered (PB) medium (pH = 7.2). Scale bar: 20 $\mu$m. The mean fluorescence intensity data are presented in SI, Figure S10b. (e) Plant cell schematic figure illustrating SW-F controlled subcellular distribution. In probenecid-free cell medium (−Pr), SW-F accumulated inside the cell vacuole. Meanwhile, the exocytosis of SW-F was stimulated *via* VMT (dashed red arrows). In presence of probenecid (+Pr), cells accumulated SW-F inside the cytoplasm and the nucleus. Meanwhile, the exocytosis was inhibited because SW-F failed to enter the cell vacuole. Washing the cells with probenecid-free medium (−Pr/w) (blue arrows, pH = 5.8) caused SW-F to redistribute into the cell vacuole. Alternatively, upon washing with PB medium (dashed red arrows, pH = 7.2), the reuptake of the exocytosed SW-F was inhibited resulting in a progressive cellular removal of SW-F. (f) Confocal microscopy images of C. roseus cell incubated in nutrient medium supplemented with 5 mM probenecid and 5 $\mu$g/mL SW-F. Cells were coincubated with the endosomal tracer FM4−64 to label endosomal organelles. The green arrows indicate red fluorescence from small endosomal organelles. The endosomal organelles could not be resolved in the bright field image because of their small size. A magnified image is reproduced in SI, Figure S11. The yellow arrows indicate green-fluoresced large resolved vesicles that lacked the red fluorescence of FM4−64. Scale bar: 10 $\mu$m. (g) Confocal microscopy images of C. roseus cell incubated in PB medium (pH 7.2, see Supplementary Text of Figure S13) and supplemented with 5 $\mu$g/mL SW-F and 5 $\mu$M Exo1. Exo1 interfered with VMT of SW-F resulting in their accumulation inside the large vesicles. The inset shows a large vesicle (arrow) containing SW-F. Scale bar: 20 $\mu$m.**

subcellular distribution mechanisms of FITC, demonstrating that the subcellular distribution of SWCNTs can be controlled by its surface functionality. Conversely, owing to their bigger size and dense characteristics, MWCNTs labeled with FITC failed to follow the probenecid-dependent distribution mechanism and therefore, their subcellular distribution became independent of surface functionality (SI, Figure S6 and Supplementary

Text). Taken together, our FRAP results were the first reported quantitative estimation of SWCNT diffusion inside living cells and they offered a unique example of how small molecules such as FITC guided the subcellular distribution of SWCNTs and were eventually released in the cell nucleus. TEM, however, could not provide direct conclusive evidence on the accumulation of SW-F in cytoplasm and nucleoplasm (SI, Figures S7 and S8).

**Control of Uptake, Subcellular Distribution and Exocytosis of Single-Walled Carbon Nanotubes (SWCNTs).** Our findings encouraged us to employ the unique uptake and distribution mechanisms of FITC (Figure 3a and SI, Figure S9) to get SWCNTs out of the cytoplasm and eventually out of the cell. A washing of probenecid-treated cells with probenecid-free cell medium (pH = 5.8) caused SW-F to redistribute into cell vacuoles ($D_{eff}$ = 49.6 $\mu m^2/s$, Figure 3b,c,e and SI, Figure S10) demonstrating that SWCNTs were cotransported with FITC *via* a CMT. Alternatively, a slight increase in washing medium pH (pH = 7.2) removed SW-F (Figure 3b,d,e and SI, Figure S10b). The removal of SW-F is believed to occur *via* a dual mechanism of a CMT followed by a vesicle-mediated transport (VMT),[25] where membrane vesicles traffic between vacuoles and plasmalemma and then release their contents to the extracytoplasmic space (Figure 3f and SI, Figure S11). Once outside the cell (pH = 7.2), the anionic form of FITC dominated the neutral form and this hampered the reuptake of SW-F through the plasmalemma resulting in a progressive removal of SW-F (Figure 3a,d,e). Similarly, the uptake of SW-F was hampered when cells were incubated with SW-F in a slightly alkaline cell medium (pH = 7.2; SI, Figure S12a). This demonstrated that the cellular uptake of SW-F can be controlled based on a change in medium pH. Alternatively, adding probenecid to the cell medium (pH = 7.2) inhibited the vacuolar transport of SW-F and resulted in their cytoplasmic accumulation (SI, Figure S12b). This indicated that entering cell vacuoles was a prerequisite for SW-F removal. To prove that VMT was the removal mechanism of SW-F, we explored the effect of Exo1[26] (an inhibitor of the ADP-ribosylation factors that play a major role in vesicle trafficking[27]). Interestingly, adding Exo1 to a cell medium interfered with vesicle trafficking and led to selective accumulation of SW-F in the large vesicles of the VMT pathway (Figure 3g and SI, Figure S13 and Supplementary Text). This labeled the vesicles with SWCNTs and highlighted the poorly understood VMT pathway.[25] Although our results provided a strategy to eliminate SWCNTs to minimize toxicity, incubating the cells in SW-F/probenecid did not show any toxicity up to 12 h (SI, Figure S14).

## CONCLUSION

In the last several decades, progress has been made for some aspects of plant biology. However, many critical areas still remain that are relatively poorly understood. First and foremost is a lack of understanding the modes of action, especially membrane trafficking and vesicle transport because study tools are currently limited to membrane-impermeable dyes.[28] The second area is the lack of organelle-targeted molecular delivery agents. Development on one of these areas is obviously dependent on advances in the other. Therefore, the major premise of this paper was to link SWCNTs as a technically important nanomaterial to cell biology basic research. This could represent a new, exciting direction that may open up new opportunities in biology and biochemistry. We illustrated the possibility of having a unique control over the subcellular distribution of the SWCNTs in the plant cell model starting from the uptake process, passing through accumulation in different subcellular structures, and ending with their cellular elimination (Figure 3e). Indeed, information about this sequence is an important prerequisite to probe and label many subcellular events. Moreover, if membrane trafficking pathways are better probed, labeled, and manipulated, then we will be in a position to understand more about cell biology and to tailor molecular delivery agents for site-specific delivery of biomolecules, especially in commercially important plant genotypes that are currently recalcitrant to genetic transformation. Furthermore, we demonstrated that SWCNTs could be involved in a CMT, which is the cornerstone of intracellular trafficking theories in both plants[21] and animals.[29] This opens a direct avenue for SWCNTs-based studies of a vast array of biological processes that are either controlled or mediated by CMT, including vacuolar transport in plants and probenecid-inhibitable vacuolar transport in macrophages.[21,30]

## EXPERIMENTAL SECTION

**Carbon Nanotubes.** Carboxylic acid functionalized single-walled carbon nanotubes (SWCNTs) were purchased from Sigma-Aldrich (St. Louis, MO, U.S.A.). These SWCNTs were >90% pure. The bundle dimensions were $D \times L$: 4−5 nm × 0.5−1.5 $\mu$m. Further shortening and oxidation of SWCNTs were performed *via* sonication and acid treatment.[17,18] Briefly, 20 mg of carboxylated SWCNTs were suspended in 20 mL 3:1 concentrated $H_2SO_4/HNO_3$ solution. The mixture was ultrasonicated for 24 h while the temperature was kept below 5 °C; this was followed by vacuum filtration through polycarbonate filter (Advantec, Dublin, CA, U.S.A.; pore size 0.1 $\mu$m). The residue was washed thoroughly with Milli-Q water, and then refluxed in 20 mL of $HNO_3$ at 120 °C overnight. After washing, FITC-labeled SWCNTs (SW-F) were prepared by mixing under sonication 1 mL SWCNTs (200 $\mu$g/mL) and 10 $\mu$L of 1 mg/mL FITC (Invitrogen, Carlsbad,

CA, U.S.A.) for 10 min at 0 °C, followed by centrifugation to remove impurities. The solution was then transferred to a dialysis film (FED, Rancho Dominguez, CA, U.S.A.; MWCO 3.5−5 KD) to remove free FITC.

**Incubation Conditions of Living Cells.** *Catharanthus roseus* cell suspension culture originating from callus culture was initiated in Murashig and Skoog medium (pH = 5.8) with minimal organics (MSMO, Sigma, St. Louis, MO, U.S.A.) supplemented with 1 $\mu$M 2,4-dichlorophenoxyacetic acid and 1 $\mu$M kinetin. Culture flasks were put in a shaker operated at 130 rpm and incubated at 25 °C in the dark. A total of 35 mL of 4-day old *C. roseus* suspension was filtered through a cell strainer (BD Falcon, Franklin Lakes, NJ, U.S.A., 70 $\mu$m Nylon) into 50 mL polypropylene test tubes and then the filtrate containing homogeneous cell suspension was centrifuged at 1000 rpm for 5 min followed by aspiration of the cell medium; this left the cells suspended in 3−5 mL of cell medium. An aliquot of 0.5 mL of the cell suspension was transferred aseptically to 2 mL plastic tubes where it was further centrifuged and washed three times with fresh MSMO and then the cells were concentrated in 50 $\mu$L MSMO. An aliquot of 300 $\mu$L of MSMO containing 5 mM probenecid[19] (Sigma, St. Louis, MO, U.S.A.) was added to the cell suspension followed by 100 $\mu$L of SW-F solution to achieve a concentration of 5 $\mu$g/mL. Probenecid was added in such a high concentration because of potential precipitation in MSMO. The precipitate was filtered prior to cell incubation. The cell suspension was then transferred to a 4-well glass slide (Lab-Tek chambers, NUNC, Rochester, NY, U.S.A.) and incubated at 25 °C for 3 h under shaking conditions (120 stroke/min). Aggregation and precipitation will occur at a high concentration of CNTs due to the salting-out effect. However, after 3 h, the cell suspension did not display visible aggregation of CNTs. A balance between MSMO and CNT concentrations was achieved to decrease the possibility of aggregation. Cells were then transferred to 2 mL plastic tubes and they were washed 3 times with fresh MSMO/probenecid medium prior to confocal microscopy and FRAP experiments. To stain the plasmalemma (Figures 1, 2, and SI, Figure S5), FM4−64 dye (Invitrogen, Carlsbad, CA, U.S.A.) was dissolved in cold phosphate buffer (pH = 7) at a concentration of 5 $\mu$g/mL. An aliquot of 10 $\mu$L of FM4−64 was added to 300 $\mu$L of washed cells and directly examined before endocytosis of the dye took place. To label the organelles of the endocytosis pathway (Figure 3 and SI, Figure 12), FM4−64 was simultaneously added with SW-F to the cell medium and then incubated for 3 h. To investigate the effect of Exo1, a stock solution was prepared at 1 mg/mL in DMSO and then Exo1 was added to the cell medium to achieve a final concentration of 5 $\mu$M.

**Confocal Microscopy Imaging of Living Cells.** A cell suspension of 300 $\mu$L was placed in glass bottom dishes (Matsunami, Kishiwada, Osaka, Japan). Live cell images were taken using 10×, 40×, and 100× objective lenses on both a laser scanning confocal microscope (Olympus, FV1000) and a super-resolution STED microscope (Leica, TCS-STED-CW). The Olympus microscope was equipped with a multiline Ar laser (458, 488, 515 nm), a HeNe(G) laser (543 nm, 1 mW), and an AOTF laser combiner plus a set of ion deposition and barrier filters. Images were acquired and analyzed using Fluoview software. The STED system was additionally equipped with a tandem scanner and a 592 nm depletion laser. To calculate the mean fluorescence intensity, the fluorescence intensities of about 300 cells were averaged.

**FRAP Experiments.** The FRAP fluorescence recovery in a photobleached area measures the diffusion rate (expressed as diffusion coefficient ($D_{eff}$)) of the fluorescent molecules, which in turn depends on the size of the macromolecular complex that contains this fluorescent label. FRAP also determines the fraction of molecules capable of recovering in the photobleached area, referred to as the mobile fraction. FRAP experiments were done with the Olympus FV1000 using the 488 nm line of a 400 mW Ar laser in conjunction with a 60× objective lens for optimum resolution (for cytoplasm and nucleus FRAP) or 10× objective lens to achieve a sufficient depth for bleaching in *z* (for vacuole FRAP). Results were also obtained on a different FRAP system Leica TCS SP5 II to confirm the original results. For qualitative experiments (Figures 1, 2, and SI, Figures S3,S4), cells were suspended in 2% low melting point agarose (Sigma, St. Louis, MO, U.S.A.) to suppress cell movement during acquisition. photobleached at full laser power (100% power, 100% transmission) and recovery of fluorescence was monitored at low laser power (30% power, 0.5% transmission). For the quantitative $D_{eff}$ measurements listed in Table 1, the fluorescence within the circles was measured at low laser power (20% power, 1−2% transmission) before and after bleaching. Recovery was followed at different sampling times and only 30−60 postbleach images were acquired to minimize photobleaching and production of artifacts. Photobleaching was corrected using the formula:

$$N_dFI = \frac{F_{bl(-)}}{F_{ref(-)}} - \frac{F_{bl(t)}}{F_{ref(t)}}$$

$N_dFI$ is the normalized difference of fluorescence intensity. $F_{bl(-)}$ is the prebleach fluorescence intensity in the bleached ROI (region of interest). $F_{ref(-)}$ is the prebleach fluorescence intensity in a reference ROI (taken in a neighboring cell or in another place within the cell at some distance from the bleach ROI). $F_{bl(t)}$ is the postbleach fluorescence intensity at time *t* in the bleach ROI. $F_{ref(t)}$ is the postbleach fluorescence intensity at time *t* in the reference ROI. The final recovery curve after photobleaching correction is an exponentially decaying function for $N_dFI$. The experimental data were fit to the following formula according to Kapitza *et al.*[31] (see Supporting Information for a justification on the use of the Kapitza model to analyze FRAP data):

$$N_dFI = A(1 - e^{-w^2/4Dt}) + B$$

*A* and *B* are the fractions of mobile and immobile components, respectively, that is, mobile fraction = $A/(A + B)$. *D* is the diffusion coefficient, *w* is the diameter of the photobleached circle in $\mu$m, and *t* is time in seconds.

*Acknowledgment.* We are grateful to Prof. E. D. Siggia (Rockefeller University, NY, U.S.A.) for providing the simulation tool for whole cell photobleaching recovery. We would like to thank Drs. K. Nitta and A. Kitayama, Terabase Inc., and Prof. K. Nagayama for their precious help with the TEM experiments performed in the microscopy facility at Okazaki Institute for Integrative Bioscience, National Institutes of Natural Sciences. We appreciate the efforts of Ms. R. Tsukamoto (Department of Applied Chemistry, Graduate School of Engineering, Nagoya University) for her assistance in preparing plant cell cultures and manipulating them. We would like to thank Mr. N. Toyohiro (Nagoya University, Japan) for providing the drawings of the plant cell. This research was partly supported by the Industrial Technology Research Grant Program from the New Energy and Industrial Technology Development Organization (NEDO) of Japan and the Japan Society for the Promotion of Science (JSPS) through its "Funding Program for World-Leading Innovative R&D on Science and Technology (FIRST Program)". This work was also supported by the "Center National de la Recherche Scientifique". M.F.S. is grateful to the JSPS for financing his Postdoctoral appointment. E.V. wishes to thank the European Union ANTICARB program (HEALTH-2007-201587) for financial support.

*Supporting Information Available:* Supplementary methods, figures, and text. This material is available free of charge *via* the Internet at http://pubs.acs.org.

## REFERENCES AND NOTES

1. Zhang, L.; Gu, F.; Chan, J. M.; Wang, A. Z.; Langer, R. S.; Farokhzak, O. C. Nanoparticles in Medicine: Therapeutic Applications and Developments. *Clin. Pharmacol. Ther.* **2008**, *83*, 761–769.
2. Cai, D.; Mataraza, J.; Qin, Z.; Huang, Z.; Huang, J.; Chiles, T.; Carnagan, D.; Kempa, K.; Ren, Z. Highly Efficient Molecular Delivery into Mammalian Cells Using Carbon Nanotube Spearing. *Nat. Methods* **2005**, *2*, 449–454.
3. Kostareleos, K.; Lacerda, L.; Pastorin, G.; Wu, W.; Sébastien, W.; Jacqueline, L.; Godefroy, S.; Pantarotto, D.; Briand, J. P.; Muller, S.; et al. Cellular Uptake of Functionalized Carbon

Nanotubes is Independent of Functional Group and Cell Type. *Nature Nanotechnol.* **2007**, *2*, 108–113.
4. Liu, S.; Wei, L.; Hao, L.; Fang, N.; Chang, M. W.; Xu, R.; Yang, Y.; Chen, Y. Sharper and Faster "Nano Darts" Kill More Bacteria: A Study of Antibacterial Activity of Individually Dispersed Pristine Single-Walled Carbon Nanotube. *ACS Nano* **2009**, *3*, 3891–3902.
5. Liu, Q.; Chen, B.; Wang, Q.; Shi, X.; Xiao, Z.; Lin, J.; Fang, X. Carbon Nanotubes as Molecular Transporters for Walled Plant Cells. *Nano Lett.* **2009**, *9*, 1007–1010.
6. Serag, M. F.; Kaji, N.; Gaillard, C.; Okamoto, Y.; Terasaka, K.; Jabasini, M.; Tokeshi, M.; Mizukami, H.; Bianco, A.; Baba, Y. Trafficking and Subcellular Localization of Multiwalled Carbon Nanotubes in Plant Cells. *ACS Nano* **2011**, *5*, 493–499.
7. Poland, C. A.; Duffin, R.; Kinloch, I.; Maynard, A.; Wallace, W. A. H.; Seaton, A.; Stone, V.; Brown, S.; MacNee, W.; Donaldson, K. Carbon Nanotubes Introduced Into The Abdominal Cavity of Mice Show Asbestos-like Pathogenecity in a Pilot Study. *Nature Nanotechnol.* **2008**, *3*, 423–428.
8. Kam, N. W.; Dai, H. Carbon Nanotubes as Intracellular Protein Transporters: Generality and Biological Functionality. *J. Am. Chem. Soc.* **2005**, *127*, 6021–6026.
9. Pantarotto, D.; Briand, J. P.; Prato, M.; Bianco, A. Translocation of Bioactive Peptides Across Cell Membranes by Carbon Nanotubes. *Chem. Commun.* **2004**, *1*, 16–17.
10. Kam, N. W.; Liu, Z.; Dai, H. Carbon Nanotubes as Intracellular Transporters for Proteins and DNA: An Investigation of the Uptake Mechanism and Pathway. *Angew. Chem., Int. Ed.* **2006**, *45*, 577–581.
11. Liu, Z.; Sun, X.; Nakayama-Ratchford, N.; Dai, H. Supramolecular Chemistry on Water-Soluble Carbon Nanotubes for Drug Loading and Delivery. *ACS Nano* **2007**, *1*, 50–56.
12. Pantarotto, D.; Singh, R.; McCarthy, D.; Erhardt, M.; Briand, J. P.; Prato, M.; Kostarelos, K.; Bianco, A. Functionalized Carbon Nanotubes for Plasmid DNA Gene Delivery. *Angew. Chem., Int. Ed.* **2004**, *43*, 5242–5246.
13. Porter, A. E.; Gass, M.; Muller, K.; Skepper, J. N.; Midgley, P. A.; Welland, M. Direct Imaging of Single-Walled Carbon Nanotubes in Cells. *Nat. Nanotechnol.* **2007**, *2*, 713–717.
14. Snapp, E. L.; Altan, N.; Lippincott-Schwartz, J. Measuring Protein Mobility by Photobleaching GFP Chimeras in Living Cells. *Curr. Protoc. Cell Biol.* **2003**, *21*, 21.1–21.1.24.
15. Deschout, H.; Hagman, J.; Fransson, S.; Jonasson, J.; Rudemo, M.; Lorén, N.; Braeckmans, K. Straightforward FRAP for Quantitative Diffusion Measurements with a Laser Scanning Microscope. *Opt. Express* **2010**, *18*, 22886–22905.
16. Makhzoum, A.; Petit-Paly, G., St; Pierre, B.; Bernards, M. A. Functional Analysis of the DAT Gene Promoter Using Transient *Catharanthus roseus* and Stable *Nicotiana tabacum* Transformation Systems. *Plant Cell Rep.* **2011**, *30*, 1173–1182.
17. Liu, J.; Rinzler, A. G.; Dai, H.; Hafner, J. H.; Bradley, R. K.; Boul, P. J.; Lu, A.; Iverson, T.; Shelimov, K.; Huffman, C. B.; Rodriguez-Macias, F.; Shon, Y.-S.; Lee, T. R.; Colbert, D. T.; Smalley, R. E. Fullerene Pipes. *Science* **1998**, *280*, 1253–1256.
18. Nakayama-Ratchford, N.; Bangsaruntip, S.; Sun, X.; Welsher, K.; Dai, H. Noncovalent Functionalization of Carbon Nanotubes by Fluorescein-Polyethylene Glycol: Supramolecular Conjugates with pH-Dependent Absorbance and Fluorescence. *J. Am. Chem. Soc.* **2007**, *129*, 2448–2449.
19. Cole, L.; Coleman, J.; Evans, D.; Hawes, C. Internalisation of Fluorescein Isothiocyanate and Fluorescein Isothiocyanatedextran by Suspension-Cultured Plant Cells. *J. Cell Sci.* **1990**, *96*, 721–730.
20. O'driscoll, D.; Wilson, G.; Steer, M. W. Lucifer Yellow and Fluorescein Isothiocyanate Uptake by Cells of *Morinda citrifolia* in Suspension Cultures is not Confined to the Endocytotic Pathway. *J. Cell Sci.* **1991**, *100*, 237–241.
21. Oparka, K. J. Uptake and Compartmentation of Fluorescent Probes by Plant Cells. *J. Exp. Bot.* **1991**, *42*, 565–579.
22. Ochs, R. L.; Lischwe, M. A.; Spohn, W. H.; Busch, H. Fibrillarin: A New Protein of the Nucleolus Identified by Autoimmune Sera. *Biol. Cell* **1985**, *54*, 123–133.
23. Moreno Díaz de la Espina, S. M. Nuclear Matrix Isolated From Plant Cells. *Int. Rev. Cytol.* **1995**, *162*, 75–139.
24. Ginisty, H.; Sicard, H.; Roger, B.; Bouvet, P. Structure and Functions of Nucleolin. *J. Cell Sci.* **1999**, *112*, 761–772.
25. Echeverría, E. Vesicle-Mediated Solute Transport Between the Vacuole and the Plasma Membrane. *Plant Physiol.* **2000**, *123*, 1217–1226.
26. Feng, Y.; Yu, S.; Lasell, T. K. R.; Jadhav, A. P.; Macia, E.; Chardin, P.; Melancon, P.; Roth, M.; Mitchison, T.; Kirchhausen, T. Exo1: A New Chemical Inhibitor of the Exocytic Pathway. *Proc. Natl. Acad. Sci. U.S.A.* **2003**, *100*, 6469–6474.
27. Lee, M. H.; Min, M. K.; Lee, Y. J.; Jin, J. B.; Shin, D. H.; Kim, D. H.; Lee, K.-H.; Hwang, I. ADP-Ribosylation Factor 1 of Arabidopsis Plays a Critical Role in Intracellular Trafficking and Maintenance of Endoplasmic Reticulum Morphology in Arabidopsis. *Plant Physiol.* **2002**, *129*, 1507–1520.
28. Šamaj, J. In *Methods and Molecular Tools for Studying Endocytosis in Plants: An Overview in Plant Endocytosis*; Šamaj, J., Baluška, F., Menzel, D., Eds.; Springer: Berlin, 2006; pp 1−17.
29. Sherwood, L. *Fundamentals of Physiology: A Human Perspective*; Thomson Brooks/Cole: Belmont, 2006; pp 55−59.
30. Steinberg, T. H.; Newman, A. S.; Swanson, J. A.; Silverstein, S. C. Macrophages Possess Probenecid-Inhibitable Organic Anion Transporters That Remove Fluorescent Dyes from The Cytoplasmic Matrix. *J. Cell. Biol.* **1987**, *105*, 2695–2702.
31. Kapitza, H. G.; McGregor, G.; Jacobson, K. A. Direct Measurement of Lateral Transport in Membranes by Using Time-Resolved Spatial Photometry. *Proc. Natl. Acad. Sci. U.S.A.* **1985**, *82*, 4122–4126.